Pattern Formation during Deformation of a Confined Viscoelastic Layer: From a Viscous Liquid to a Soft Elastic Solid

Julia Nase and Anke Lindner*

Laboratoire de Physique et Mécanique des Milieux Hétérogènes (PMMH), UMR 7636, CNRS - ESPCI - Universités Paris 6 et 7, 10, rue Vauquelin, 75231 Paris Cedex 05, France

Costantino Creton

Laboratoire de Physico-Chimie des Polymères et des Milieux Disperses (PPMD), UMR 7615, CNRS - ESPCI -Universités Paris 6 et 7, 10 rue Vauquelin, 75231 Paris Cedex 05, France

(Received 23 April 2008; published 14 August 2008)

We study pattern formation during tensile deformation of confined viscoelastic layers. The use of a model system [poly(dimethylsiloxane) with different degrees of cross-linking] allows us to go continuously from a viscous liquid to an elastic solid. We observe two distinct regimes of fingering instabilities: a regime called ''elastic'' with interfacial crack propagation, where the fingering wavelength scales only with the film thickness, and a bulk regime called ''viscoelastic,'' where the fingering instability shows a Saffman-Taylor-like behavior. We find good quantitative agreement with theory in both cases and present a reduced parameter describing the transition between the two regimes and allowing us to predict the observed patterns over the whole range of viscoelastic properties.

DOI: 10.1103/PhysRevLett.101.074503 PACS numbers: 47.54.−r, 47.20.Gv, 68.15.+e, 83.80.Va

Introduction.—Good soft adhesives show viscous and elastic properties that allow having, on the one hand, a good molecular contact with the substrate and, on the other hand, a resistance to a certain stress level during debonding. The viscoelastic properties determine the debonding mechanisms when being detached from a rigid substrate, involving the formation of complex patterns as bulk fingering or interfacial crack propagation [1]. Pattern formation during tensile deformation of thin layers in confined geometries has also attracted much interest from a fundamental point of view. In the case of a purely viscous liquid confined between two plates being separated, air penetrating from the edges leads to the formation of bulk fingers. This fingering instability is well described by the classical Saffman-Taylor instability [2–7], where a less viscous liquid pushes a more viscous liquid in a confined geometry. For a thin layer of a purely elastic material, undulations of an interfacial crack front have been observed experimentally and explained theoretically [8–11]. Some studies have focused on complex or yield stress fluids [4,5], elastic gels [12,13], ferromagnetic fluids [14], and pastes [15] or considered the role of the substrate [16]. The transition between a viscous liquid and a glassy material has been studied [17,18].

However, no systematic study of the pattern formation during deformation of a viscoelastic material focusing on the respective role of the liquid and elastic properties has been undertaken so far. We present here a system involving a specifically designed model soft material with tunable properties going continuously from a viscous liquid to an elastic solid. Studying the debonding mechanisms using a probe tack test on these materials allows us for the first time to explain the observed patterns quantitatively over the whole range of viscoelastic properties and to describe the transition between the two well known limits observed for a pure liquid or an elastic solid. Such a study helps for a better understanding of the instabilities observed in the viscoelastic regime of industrial applications. It is also of importance for any theoretical treatment aiming to bridge the gap between the different formalisms that apply to viscous liquids and elastic solids.

Materials and methods.—As a model system, we use a weakly cross-linked polymer, poly(dimethylsiloxane) (PDMS). We chose the commercial product ''Sylgard© 184 Silicone Elastomer Kit'' purchased at Dow Corning. It consists of a silicone oil and a curing agent that is able to form cross-links, i.e., chemical bonds between the polymer chains. The noncured silicone oil is a Newtonian liquid. Adding a curing agent increases the number density of cross-link points, and the material becomes viscoelastic. The fully cured PDMS at 10% of curing agent is an elastic solid. This system thus represents an ideal model system providing a reproducible and easy way to go continuously from a viscous liquid to an elastic solid.

To determine the material's linear rheological properties, we perform oscillatory frequency sweep tests after curing in a plate-plate geometry. This gives access to the storage and loss moduli G' and G'' that are measures for the material's elastic and viscous properties, respectively, as well as to the complex modulus $G^\star = \sqrt{G'^2 + G''^2}$.

Figure 1 shows the results for different amounts of cross-linker. The material with about 3% of cross-linker is elastic, having a G' several orders of magnitude higher than G''; adding about 1% of cross-linker leads to a product in the viscoelastic regime close to the gel point.

We prepare polymeric films on microscope glass slides ($10 \times 2.6 \times 0.2$ cm) that are precleaned and coated with a primer (Dow Corning 1200 OS) to enhance the adherence

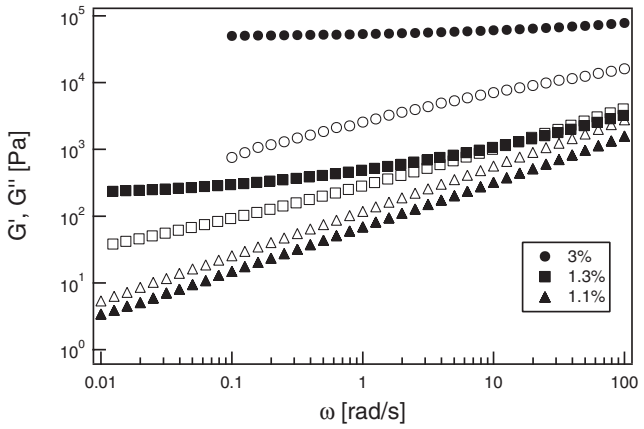

FIG. 1. The storage and loss moduli G' (solid symbols) and G'' (open symbols) as a function of the frequency ω for different amounts of curing agent.

of PDMS to the slide. We use applicators to deposit films of different thicknesses. The samples are cured in a desiccator at 80 °C for five hours under vacuum. To determine the final thickness, we measure the film's weight and size. We validated this method by comparison with an optical technique using interference fringes.

We perform tensile deformation tests using a homebuilt "probe tack" setup with good resolution and visualization capabilities [19]. It mainly consists of a flat circular steel probe that is brought into contact and debonded from a soft viscoelastic film with controlled speed; see Fig. 2. During the test, the probe displacement and the normal force on the probe are measured. We also visualize the debonding process from above with a camera mounted on a microscope to gain qualitative insight into the debonding mechanisms. The probe has a radius $R = 3$ mm and is made of polished stainless steel.

Experimental.—The parameters varied in our experiments, besides the viscoelastic properties, are the layer thickness b and the debonding speed v. Typical values are $b = 50$–500 μm and $v = 1$–200 μm/s. During a typical experiment, air penetrates from the edge of the confined layer. It can penetrate either in the bulk, followed by a strong deformation and the subsequent formation of thin "bridges" (fibrils) between the probe and the glass slide, or at the interface between the probe surface and the polymer film, leading to a fast debonding by interfacial crack propagation. In both cases, we observe the destabilization of the initially circular debonding line by undulations and the subsequent propagation of air fingers. We characterize the emerging patterns by determining the finger number n at the moment the first undulations are observable (see the inset in Fig. 5) and calculate a wavelength $\lambda = 2\pi R/n$. Initially, a destabilizing wavelength can be clearly defined, but as the time and debonding process go on, highly nonlinear patterns are evolving, showing features such as side branching and tip splitting; see Fig. 3. In the present study, we restrict our interest to the analysis of the linear destabilization process at the onset.

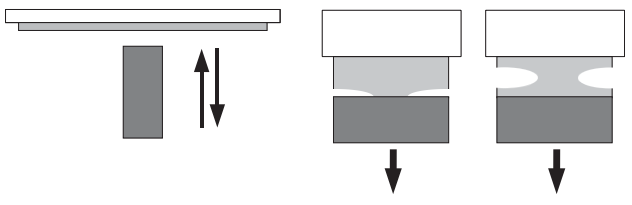

FIG. 2. Left side: Schematic view of the "probe tack" experiment. Right side: Interfacial crack propagation and bulk deformation mechanisms.

Results and discussion.—We characterize here in more detail the two cases of interfacial and bulk mechanisms introduced above. Although the patterns look quite similar in the top view pictures in Figs. 3(a) and 3(b), two different mechanisms are at their origin.

In the case of the viscoelastic regime characterized by fibrillation and a bulk deformation mechanism, the pattern formation is sensitive to both the initial film thickness and the debonding speed for a given material. As the wavelength decreases with the debonding speed and increases linearly with the initial film thickness [Fig. 4(a)], one can attempt to compare λ to the classical Saffman-Taylor (ST) or viscous fingering instability [2,20] predicting by linear stability analysis

$$\lambda = \pi b/\sqrt{\mathrm{Ca}}. \tag{1}$$

$\mathrm{Ca} = U\eta/\sigma$ is the dimensionless capillary number comparing viscous to capillary forces, η is the viscosity, $\sigma = 20$ mN/m is the surface tension between PDMS and air, and U denotes the radial velocity of the circular interface. Presuming an incompressible fluid and therefore volume conservation, $U = Rv/2b$ for a Newtonian fluid. To adapt this prediction to the case of viscoelastic materials, we replace the Newtonian viscosity with a complex viscosity $|\eta^\star|$ defined as $G^\star/\omega$. $|\eta^\star|$ depends on the frequency, estimated for each of our experiments following $\omega = 2\pi U/b$.

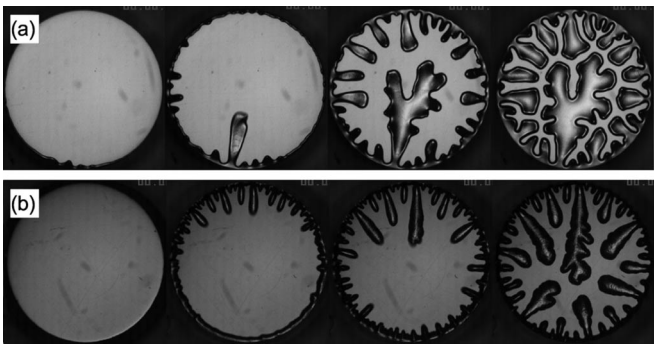

FIG. 3. Formation of air fingers in the elastic and viscoelastic cases: (a) interfacial crack propagation and (b) bulk deformation.

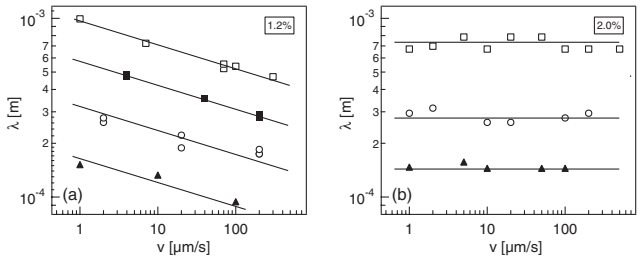

FIG. 4. Left side, viscoelastic case: λ depends on b and v. $\square = 350\ \mu$m, $\blacksquare = 230\ \mu$m, $\bigcirc = 120\ \mu$m, and $\blacktriangle = 60\ \mu$m. Right side, elastic case: λ depends only on b. $\square = 300\ \mu$m, $\bigcirc = 130\ \mu$m, and $\blacktriangle = 70\ \mu$m. The black lines are a guide for the eye.

Figure 5 shows a good quantitative agreement between the ST prediction and our data, despite some scattering. The limit of a purely viscous liquid is represented by the dark full spots obtained for Newtonian silicone oils [21]. Surprisingly, the ST prediction holds going from the viscous limit up to highly non-Newtonian viscoelastic materials above the gel point.

The second case that we investigated, the elastic regime, is characterized by interfacial crack propagation. The linear wavelength does not depend on the debonding speed over three decades; see Fig. 4(b). The dependence on the debonding speed is a quantitative criterion to decide to which regime an experiment belongs. Figure 6 shows that λ depends only on the initial film thickness b over 3 orders of magnitude of the elastic modulus ($1\ \text{kPa} \lesssim G' \lesssim 0.5\ \text{MPa}$). These results are in qualitative agreement with theoretical predictions and with experimental observations in a slightly different geometry [8]. Linear stability analysis has also been done by Adda-Bedia and Mahadevan [9]. Considering the case of static peeling, they take into account the bending stiffness of the flexible cover plates used for the peeling tests and the finite film thickness. They calculate a critical confinement above which shear deformations are more beneficial for the system's energy than normal deformations, leading to undulations. The confinement parameter α is defined as $(D/Eb^3)^{1/3}$, D being the bending stiffness of the cover plate, E the film's elastic modulus, and b the film thickness. The critical value $\alpha_c \simeq 21$ is in good agreement with experiments by Ghatak *et al.*, who find $\alpha_c \simeq 18$. We compare our experiments to these results by considering the bending stiffness of our microscopic glass slides. With $D \simeq 70\ \text{N m}$ for a glass slide of $b = 2$ mm, we find $\alpha > 70$ for all of our experiments; thus, we place ourselves always in the regime of an unstable crack front. The critical wavelength calculated in Ref. [9] $\lambda_c \simeq 3.4b$ scales only with the film thickness and is independent of all material parameters. Our result $\lambda = 2.3b$ is in good quantitative agreement with theory. Deviations might be due to the fact that calculations are done for $\alpha = \alpha_c$, whereas our experiments are placed far beyond the critical value.

A surprising result of our work is the very abrupt change in the debonding behavior: Our experiments always fall into the elastic or viscoelastic regime without experiencing a transition regime. The appropriate parameter to describe the transition between interfacial and bulk mechanisms in the case of an elastic rubber has been proposed to be $\mathcal{G}_c/Eb$ [13]. The critical energy release rate $\mathcal{G}_c$ is a measure for the energy that one has to provide to the system to make an interfacial crack move. Eb represents the elastic energy necessary to deform the bulk of a sample of thickness b with elastic modulus E. For a viscoelastic material, $\mathcal{G}_c$ can be divided into a constant component $\mathcal{G}_0$, the threshold fracture energy, and a dissipation term depending on crack velocity. It has been proposed [22] that the dissipation term should be proportional to $\tan\delta = G''/G'$. Hence, approximating $\mathcal{G}_c \sim \mathcal{G}_0 \tan\delta$ and substituting into $\mathcal{G}_c/Eb$ yields for soft viscoelastic layers a new parameter $(\mathcal{G}_0 \tan\delta)/(G'b)$ depending only on the linear rheological

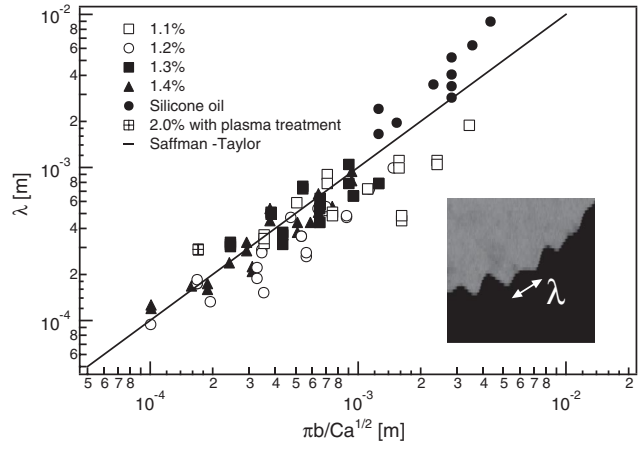

FIG. 5. In the viscoelastic case, the wavelength scales linearly with the thickness and is inversely proportional to the square root of the capillary number.

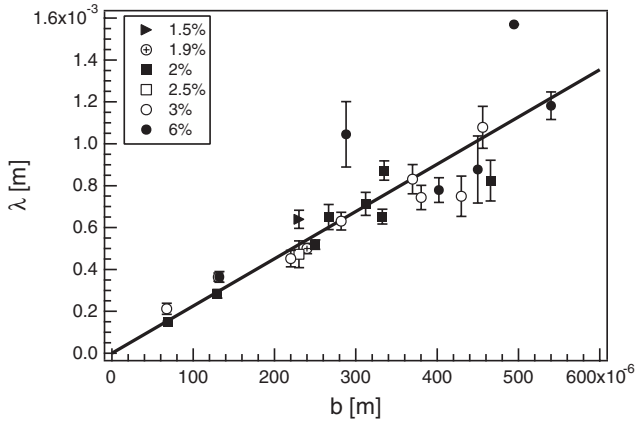

FIG. 6. In the case of interfacial crack propagation, the wavelength scales only with the thickness b. The solid line is a straight line fit to the data yielding $\lambda = 2.3b$.

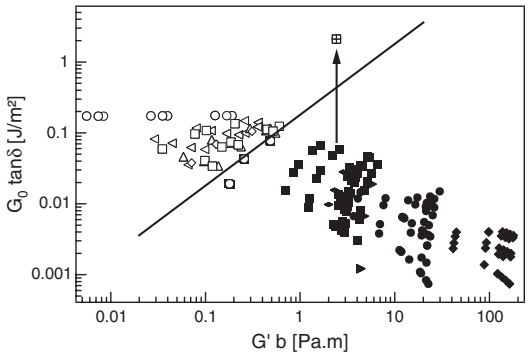

FIG. 7. Open symbols represent bulk deformation and black solid symbols interfacial crack propagation. Experiments right at the transition can show both mechanisms due to fluctuations in the sample preparation.

properties and $\mathcal{G}_0$ [23]. For cases where the energy cost to propagate a crack is high, bulk mechanisms are expected, while interfacial crack propagation should be observed when the elastic deformation of the layer requires high energy. This is well presented by plotting the parameter space spanned by $(\mathcal{G}_0 \tan\delta)$ and $(G'b)$; see Fig. 7. Solid symbols indicate interfacial and open symbols bulk mechanisms.

Following the theory, it should be possible to switch between an interfacial and a bulk mechanism by changing $\mathcal{G}_0$. We performed an exemplary experiment replacing the steel probe ($\mathcal{G}_0 \simeq 0.1$ J/m^2) by a glass surface previously subjected to plasma treatment, increasing $\mathcal{G}_0 \simeq 15$ J/m^2 considerably. We estimated $\mathcal{G}_0$ by measuring the work of adhesion for the fully cured PDMS performing a tack test at low debonding speed. We were indeed able to change the debonding mechanism from interfacial to bulk behavior for a sample with 2% of cross-linker. This experiment is represented by the symbol ⊞ in Fig. 7. Furthermore, changing $\mathcal{G}_0$ changes the wavelength which is now well described by the ST prediction; see ⊞ in Fig. 5.

Conclusion.—We present in this Letter for the first time a systematic study of the transition between bulk deformation mechanisms and interfacial crack propagation during tensile tests on thin layers of viscoelastic materials with properties going from a viscous liquid to an elastic solid. In both cases, we characterize the emerging fingering patterns quantitatively following theoretical predictions. The transition that we observe is very sharp without experiencing an intermediate regime. We propose a possible empirical parameter that allows us to draw a mechanism map spanned by the parameters $\mathcal{G}_0 \tan\delta$ and $G'b$ separating nicely the different mechanisms and allowing us therefore to predict the debonding behavior of our system.

We thank Mokhtar Adda-Bedia, Arezki Boudaoud, and Dominic Vella (LPS-ENS) for stimulating discussions and Guylaine Ducouret (PPMD-ESPCI) and Alexis Prevost (LPS-ENS) for help with the sample characterization.

*anke.lindner@espci.fr

[1] K. R. Shull and C. Creton, J. Polym. Sci. B **42**, 4023 (2004).
[2] P. G. Saffman and G. Taylor, Proc. R. Soc. A **245**, 312 (1958).
[3] A. Lindner, D. Derks, and M. J. Shelley, Phys. Fluids **17**, 072107 (2005).
[4] D. Derks, A. Lindner, C. Creton, and D. Bonn, J. Appl. Phys. **93**, 1557 (2003).
[5] M. Ben Amar and D. Bonn, Physica (Amsterdam) **209D**, 1 (2005).
[6] M. J. Shelley, F. R. Tian, and K. Wlodarski, Nonlinearity **10**, 1471 (1997).
[7] S. Poivet, F. Nallet, C. Gay, J. Teisseire, and P. Fabre, Eur. Phys. J. E **15**, 97 (2004).
[8] A. Ghatak, M. K. Chaudhury, V. Shenoy, and A. Sharma, Phys. Rev. Lett. **85**, 4329 (2000); V. Shenoy and A. Sharma, Phys. Rev. Lett. **86**, 119 (2001); A. Ghatak and M. K. Chaudhury, Langmuir **19**, 2621 (2003); A. Ghatak and M. K. Chaudhury, J. Adhes. **83**, 679 (2007).
[9] M. Adda-Bedia and L. Mahadevan, Proc. R. Soc. A **462**, 3233 (2006).
[10] W. Monch and S. Herminghaus, Europhys. Lett. **53**, 525 (2001).
[11] R. J. Fields and M. F. Ashby, Philos. Mag. **33**, 33 (1976).
[12] K. R. Shull, C. M. Flanigan, and A. J. Crosby, Phys. Rev. Lett. **84**, 3057 (2000).
[13] R. E. Webber, K. R. Shull, A. Roos, and C. Creton, Phys. Rev. E **68**, 021805 (2003).
[14] R. M. Oliveira and J. A. Miranda, Phys. Rev. E **73**, 036309 (2006).
[15] H. Lemaire, Y. Ould Mohamed Abdelhaye, J. Larue, R. Benoit, P. Levitz, and H. Van Damme, Fractals **1**, 968 (1993).
[16] S. Sinha, T. Dutta, and S. Tarafdar, Eur. Phys. J. E **25**, 267 (2008).
[17] J. A. F. Harvey and D. Cebon, J. Mater. Sci. **38**, 1021 (2003).
[18] B. X. Zhao, H. B. Zeng, Y. Tian, and J. Israelachvili, Proc. Natl. Acad. Sci. U.S.A. **103**, 19 624 (2006); H. Zeng, Y. Tian, B. Zhao, M. Tirrell, and J. Israelachvili, Macromolecules **40**, 8409 (2007).
[19] G. Josse, P. Sergot, C. Creton, and M. Dorget, J. Adhes. **80**, 87 (2004).
[20] L. Paterson, J. Fluid Mech. **113**, 513 (1981).
[21] D. Derks and A. Lindner (private communication).
[22] D. Maugis and M. Barquins, J. Phys. D **11**, 1989 (1978).
[23] C. Carelli, F. Deplace, L. Boissonnet, and C. Creton, J. Adhes. **83**, 491 (2007).